Pharmaceutical Biotechnology

Recombinant Subunit Rotavirus Trivalent Vaccine Candidate: Physicochemical Comparisons and Stability Evaluations of Three Protein Antigens

Check for updates

Sanjeev Agarwal [1], John M. Hickey [1], Neha Sahni [1], Ronald T. Toth IV [1], George A. Robertson [2], Robert Sitrin [2], Stanley Cryz [2], Sangeeta B. Joshi [1], David B. Volkin [1, *]

[1] Department of Pharmaceutical Chemistry, Vaccine Analytics and Formulation Center, University of Kansas, Lawrence, Kansas 66047
[2] The Center for Vaccine Innovation and Access, PATH, Washington, District of Columbia 20001

ARTICLE INFO

ABSTRACT

Although live attenuated *Rotavirus* (RV) vaccines are available globally to provide protection against enteric RV disease, efficacy is substantially lower in low- to middle-income settings leading to interest in alternative vaccines. One promising candidate is a trivalent nonreplicating RV vaccine, comprising 3 truncated RV VP8 subunit proteins fused to the P2 CD4$^+$ epitope from tetanus toxin (P2-VP8-P[4/6/8]). A wide variety of analytical techniques were used to compare the physicochemical properties of these 3 recombinant fusion proteins. Various environmental stresses were used to evaluate antigen stability and elucidate degradation pathways. P2-VP8-P[4] and P2-VP8-P[6] displayed similar physical stability profiles as function of pH and temperature while P2-VP8-P[8] was relatively more stable. Forced degradation studies revealed similar chemical stability profiles with Met^1 most susceptible to oxidation, the single Cys residue (at position 173/172) forming intermolecular disulfide bonds (P2-VP8-P[6] was most susceptible), and Asn^7 undergoing the highest levels of deamidation. These results are visualized in a structural model of the nonreplicating RV antigens. The establishment of key structural attributes of each antigen, along with corresponding stability-indicating methods, have been applied to vaccine formulation development efforts (see companion paper), and will be utilized in future analytical comparability assessments.

Introduction

Rotavirus (RV) is a leading cause of acute diarrhea and gastroenteritis among infants and young children across the world with approximately 215,000 children under 5 years of age dying from RV infection each year.[1] Most deaths occur in developing countries. Furthermore, millions of children worldwide require home care, ER visits, and hospitalization, which contribute significantly to the disease burden.[2] Improvements in sanitation, personal hygiene, or food quality reduce but do not eliminate the risk of this infection.[3,4] Therefore, vaccination is the most cost-effective strategy to control the burden of RV-related illness.

Currently, 4 WHO prequalified, live attenuated oral RV vaccines (RotaTeq®, Rotarix®, Rotavac®, Rotasil®) are commercially available and combined cover more than 100 countries. In general, widely used RV vaccines (RotaTeq® and Rotarix®) show good efficacy (>85%) in developed countries, however, efficacy is reduced (40%-60%) in the low-income countries where the need is most.[5-10] Although the causes for their reduced efficacy are unknown, and are an active area of investigation, contributing factors possibly include lower viral titer (transplacentally acquired RV antibodies, components of breast milk and stomach acid) and impaired immune response (malnutrition, interfering microbes, and other coinfections).[11-13] From limited available data, lower efficacy in

certain subpopulations of the developing world of other live, attenuated oral vaccines has also been observed against enteric pathogens such as poliovirus and *Vibrio cholera.*[14] Thus, there is interest in developing recombinant subunit protein, injectable RV vaccine candidates to address some of the current deficiencies of live attenuated oral vaccination.[15]

To this end, a candidate recombinant protein−based, parenterally administered RV vaccine is under development (non-replicating RV vaccine [NRRV]). In a phase 1 clinical trial conducted in infants and toddlers in South Africa, a monovalent NRRV vaccine containing aluminum-adjuvanted P[8] antigen was shown to be well-tolerated and immunogenic, thus demonstrating a promising approach to develop a new vaccine against RV.[16,17] Moreover, a trivalent version of the aluminum-adjuvanted NRRV vaccine is currently being evaluated in infants and toddlers in early stage clinical trials in South Africa.[16] The trivalent NRRV vaccine candidate is composed of 3 recombinant protein antigens designed to protect against the most prevalent RV strains in the developing world (P[4], P[6], and P[8]).

Each of these 3 antigens is a recombinant fusion protein based on the RV surface protein VP4. Upon host infection, VP4 is cleaved by proteases in the intestinal lumen into VP5* and VP8* leading to production of neutralizing antibodies.[18] Wen et al. at the NIH successfully expressed ΔVP8*, a truncated, soluble version of the VP8* protein, in *E. coli* while preserving its key epitopes. The tetanus toxoid CD4+ T cell epitope (P2) was added on the N-terminus via a GSGSG linker to create a fusion protein which enhanced the immunogenicity of ΔVP8* as demonstrated in guinea pigs.[19] In terms of nomenclature, the 3 recombinant protein antigens are P2-VP8-P[4], P2-VP8-P[6], and P2-VP8-P[8], where P2 stands for the carrier protein, VP8 refers to the ΔVP8* part of VP8* protein, and P [4], P[6], and P[8] represent the RV strain DS-1 (G2P[4]), 1076 (G2P [6]), and Wa (G1P[8]), respectively.[20] For simplicity, the protein antigens are referred to as P[4], P[6], or P[8], respectively, in this work (see main text for further discussion).

Successful development and eventual commercialization of this recombinant subunit RV vaccine candidate will not only depend on clinical safety and efficacy results, but also the ability to produce the vaccine at low cost for use in the developing world. To this end, demonstrating a product candidate retains its critical quality attributes (CQAs, i.e., key aspects of structural integrity, stability, and immunological potency) as the manufacturing process is changed and scaled-up to ensure low-cost production is a key aspect to its development. To ensure CQAs are retained pre- versus post-process change, it is important to develop analytical assays that are robust and sensitive to detect changes in the physicochemical and immunological properties of the protein antigen. Thus, it is essential to develop a battery of analytical assays capable of monitoring structural and functional equivalence during comparability assessments.[21-23] In addition, these analytical characterization methods can be applied to the formulation development to ensure vaccine potency (and physicochemical stability) of the 3 NRRV antigens across the vaccine's shelf life.[24-26]

The work presented in here, along with an accompanying companion paper, describes physicochemical characterization, forced degradation, and formulation development studies of the 3 NRRV recombinant fusion proteins as bulk vaccine antigens. In this work, a wide variety of physicochemical characterization techniques were used to characterize and compare the primary and higher-order structures, post-translational modifications, conformational stability, and aggregation propensity of each of the 3 NRRV antigens. In addition, forced degradation studies were performed to compare physical stability profiles as a function of pH and temperature as well as to elucidate chemical degradation pathways to identify chemically labile residues (i.e., "weak spots").

Analytical tools were developed to monitor or quantify degradative changes and the most informative assays for each structural attribute will be applied to formulation development and future comparability assessments. In a companion paper, the 3 NRRV antigens are further characterized in terms of formation of aggregates and particles (e.g., counting, sizing, and physicochemical attributes) during agitation and freeze-thaw stresses. In addition, formulation development studies are described to identify candidate formulations to minimize protein aggregation and particle formation during frozen storage of these NRRV antigens as a bulk drug substance (see companion paper by Agarwal et al.[27]).

Materials and Methods

The P[4] and P[6] antigens were produced and purified from *E. coli* at Walter Reed Army Institute of Research, MD, and provided in 0.5 mM sodium phosphate, 150 mM NaCl, pH 7.2. The P[8] antigen was produced and purified from *E. coli* by Blue Sky Bio-Services, MA, and provided in 600 mM ammonium sulfate, 50 mM Tris, pH 7.5 buffer. Unless otherwise noted, each of the antigens was dialyzed overnight at 4°C in 10 mM sodium phosphate, 150 mM NaCl, pH 7.2 buffer which is referred as formulation buffer in the text hereafter. Sodium phosphate dibasic heptahydrate, and sodium chloride were purchased from Thermo Fisher Scientific (Waltham, MA). All other buffer reagents and chemicals including sodium phosphate monobasic monohydrate, citric acid, and ammonium bicarbonate were purchased from Sigma-Aldrich (St. Louis, MO) and were of analytical grade or higher unless noted otherwise. The extinction coefficient of each NRRV antigen was calculated from the primary sequence using online ExPASy tool (Swiss Institute of Bioinformatics), resulting in values of 1.653 mg/ mL^{-1} cm^{-1}, 1.708 mg/mL^{-1} cm^{-1}, and 1.733 mg/mL^{-1} cm^{-1} for P[4], P[6], and P[8] antigen, respectively, to determine protein concentration. It should be pointed out that the protein samples used in this study are bulk and by inference do not represent the aluminum-adjuvanted drug product vaccine.

Descriptions of many of the analytical methods used in this work have been published previously,[21,28,29] and detailed descriptions for all methods in this work are provided in the Supplemental Methods section. These methods include intact mass spectrometry (MS), LC-MS peptide mapping, Fourier transform infrared (FTIR) spectroscopy, far-UV circular dichroism (CD) spectroscopy, fluorescence spectroscopy, SDS-PAGE, size-exclusion chromatography, sedimentation velocity analytical ultracentrifugation, reversed-phase (RP) ultra-high pressure chromatography, hydrophobic interaction chromatography (HIC), differential scanning calorimetry, extrinsic fluorescence spectroscopy (DSF), and OD_{350} (turbidity) analysis. Experimental details for physical stability assessments using radar plots, chemical stability studies under forced degradation conditions, and structural modeling using I-TASSER are also described in the Supplemental Methods section.

Results

Physicochemical Characterization and Comparisons of the Three NRRV Antigens

The primary structure of the 3 fusion proteins was initially assessed by intact mass analysis. As shown in Figure 1, panels A, B, and C, predominantly a single peak was observed for each antigen and the average molecular weight results (20,517.6 ± 0, 20,732.0 ± 0, 20,433.7 ± 0.1 Da for P[4], P[6], and P[8], respectively, $n = 3$) correspond to the expected native protein mass based on the amino acid sequence plus an additional +132 Da (similar results were obtained for non-reduced samples, see Supplemental Fig. S1A). As
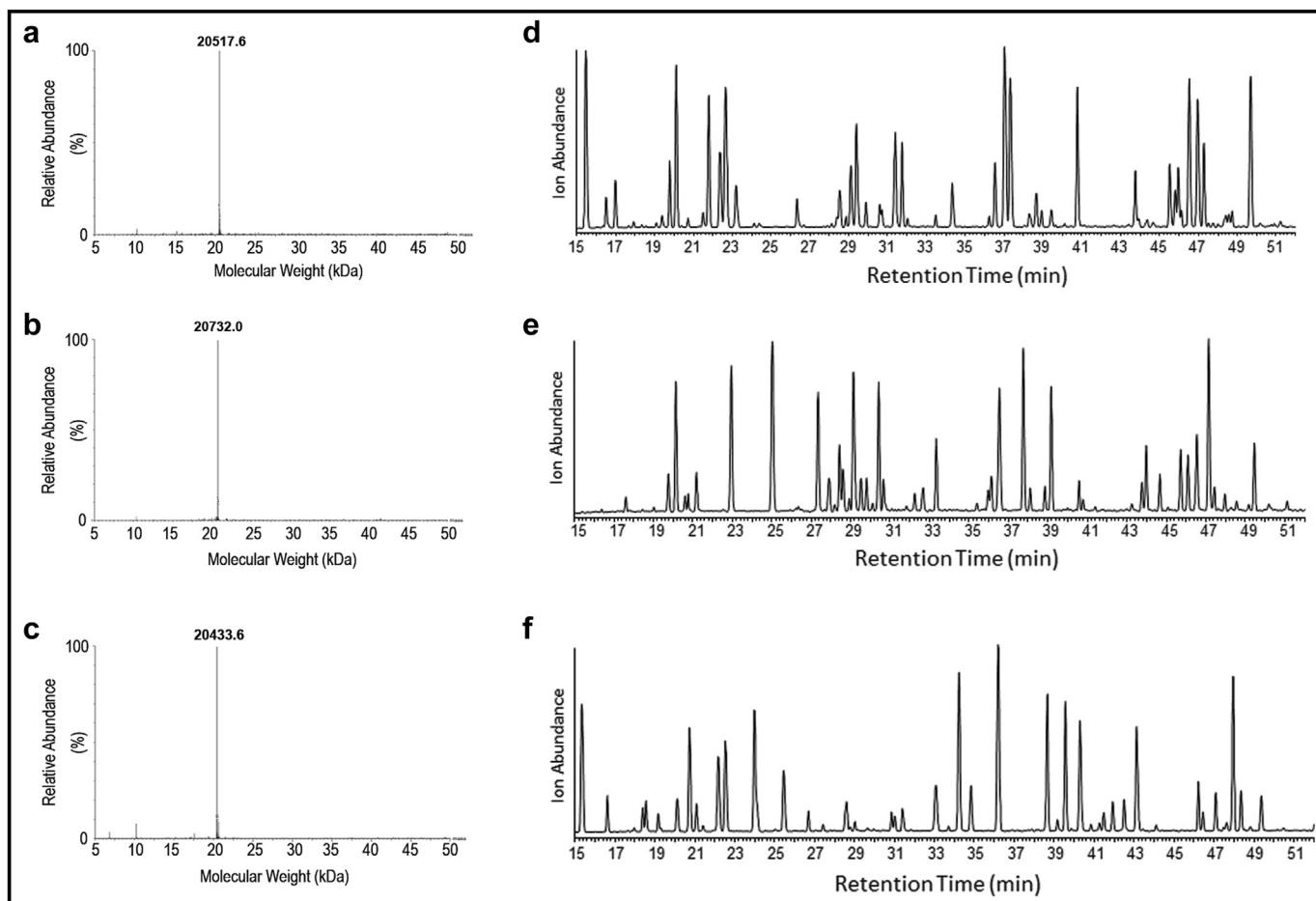
Figure 1. Primary structure analysis of the 3 NRRV antigens. Representative deconvoluted mass spectra for analysis of intact proteins under reducing condition for (a) P[4], (b) P[6], and (c) P[8]. Representative total ion chromatogram from peptide map analysis of reduced, alkylated, and chymotrypsin digested proteins for (d) P[4], (e) P[6], and (f) P[8]. See Supplemental Figure S1 for intact mass analysis data under nonreducing condition and sequence coverage (100% for both reducing and nonreducing conditions) from peptide map analysis.

confirmed by LC-MS peptide mapping results described below, an additional Met residue is present on the N-terminus of these antigens, as would be expected for a foreign protein expressed in *E. coli*.

LC-MS peptide map analysis was conducted to confirm each antigen's primary sequence and identify any posttranslational modifications. Each antigen displayed a unique peptide elution profile as shown in Figure 1 panels D, E, and F, demonstrating the ability to distinguish the 3 proteins as a potential identity test. Using intact (MS^1) and fragmentation (MS^2) mass analysis, 44 peptides were identified in the P[4] digest, 50 peptides in P[6], and 37 peptides in P[8], which covered 100% of each of the protein's primary sequence (Supplemental Fig. S1B). Moreover, the peptide mapping results suggested deamidation at several Asn residues in P[4] and P[8], and at 1 Asn residue in P[6]. For P[4], Asn^7, Asn^{47}, and Asn^{179} were ~3%-4% deamidated. For P[6], Asn^7 was ~2%-3% deamidated. For P[8], Asn^7 was ~20%, Asn^{46} ~6%, and Asn^{178} ~3% deamidated. Thus, the peptide mapping method was shown to be useful not only as an overall fingerprint analysis for the structural integrity and identity of each NRRV antigen, but also as charge heterogeneity test for Asn deamidation (also see chemical stability section below).

The overall higher-order structure (HOS) of the 3 proteins was assessed by a combination of different biophysical tools. The secondary structure composition was measured by FTIR by monitoring the absorbance in the amide I region (1600-1700 cm^{-1}). All 3 antigens were primarily β-sheet in structure with main peak at ~1642, ~1639, and ~1640 cm^{-1} for P[4], P[6], and P[8], respectively, as shown in Figure 2, panels A, B, and C. The secondary structure composition by Fourier self-deconvolution (see Fig. 2d) correlated very well with the secondary structure assignments from X-ray crystal structures of P[4] and P[8] antigens in the literature.[30,31] Far-UV circular dichroism spectroscopy was used to confirm the findings from FTIR analysis and a peak minimum around 215-216 nm was observed for each antigen indicating β-sheet structure in solution (Fig. 2e). The overall tertiary structure was compared using intrinsic tryptophan fluorescence emission spectrum from 305 to 405 nm. Peak position or λ_{max} for P[4], P[6], and P[8] was 334 ± 0, 333.7 ± 0.6, and 335.3 ± 0.6, respectively (Fig. 2f). This result suggests the average Trp residue for each of the 3 antigens is located in a similar environment (each NRRV antigen has 4 Trp residues).

A combination of sedimentation velocity analytical ultracentrifugation and size exclusion-high performance liquid chromatography (SE-HPLC) were used to probe the size of the 3 protein antigens and to assess the presence of soluble aggregates (monomer, dimer, etc.). Each antigen had monomeric composition ≥99% and about 1% higher molecular weight (HMW) species based on the peak areas from sedimentation coefficient (s) distribution (Fig. 3a). Similar s value of 2.09 ± 0.01 was recorded for P[4] and P[8], whereas for P[6], s value was 2.03 ± 0.01 suggesting smaller
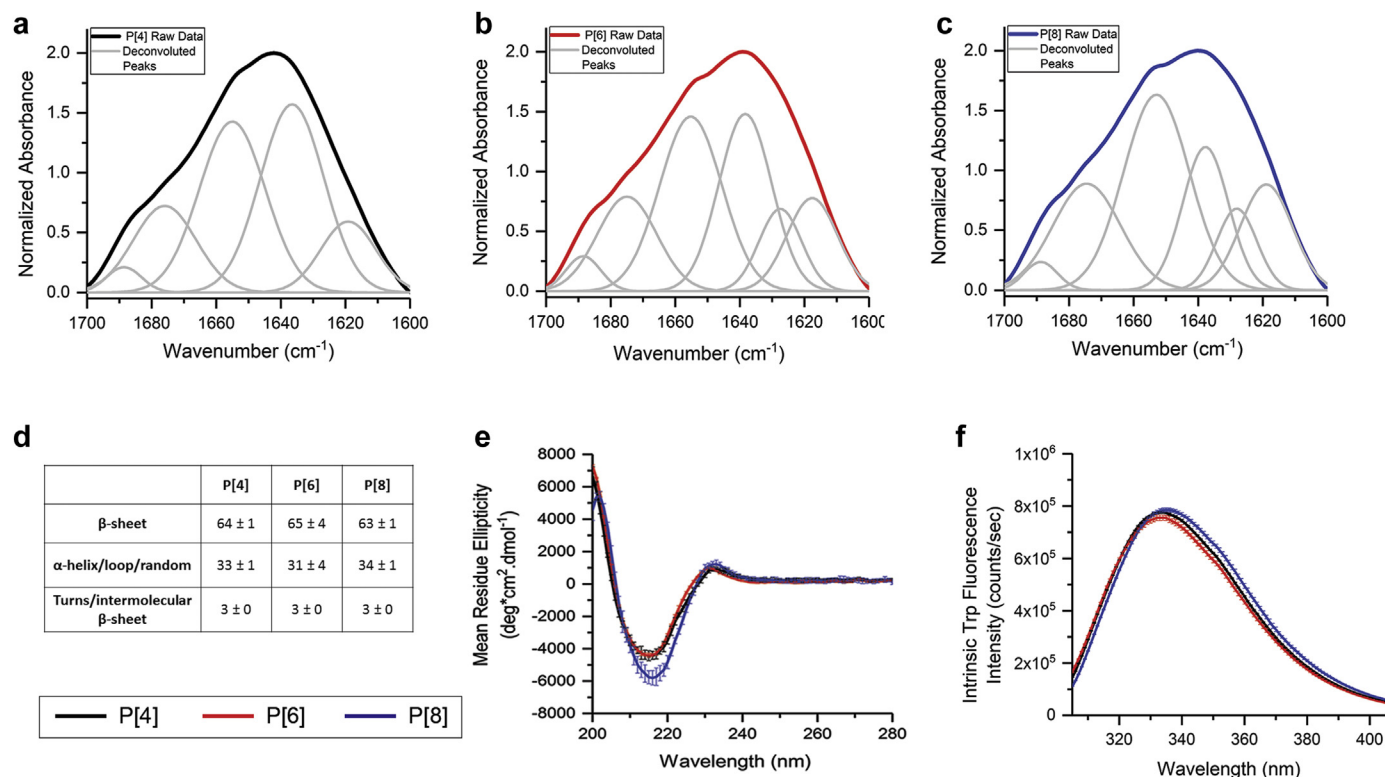
Figure 2. Higher-order structure (HOS) analysis of each of the 3 NRRV protein antigens at 10°C in 10 mM PBS, pH 7.2. Representative FTIR absorbance spectrum of the amide I region and Fourier self-deconvoluted peaks for (a) P[4], (b) P[6], (c) P[8] antigens, and (d) secondary structure composition of each antigen obtained from Fourier self-deconvolution of FTIR spectrum. (e) Far-UV CD spectra and (f) intrinsic tryptophan fluorescence emission spectra overlay for the 3 antigens. Error bars denote 1SD from triplicate measurements.

hydrodynamic size for P[6] compared to P[4] and P[8] (which show similar size). These observations were supported by SE-HPLC as an orthogonal tool. The retention time for P[4] and P[8] was 16.28 ± 0.01 and 16.24 ± 0.01 min, respectively, whereas P[6] eluted at 17.08 ± 0.06 min consistent with a smaller hydrodynamic size for P [6] (Fig. 3b). As expected based on the size results from intact mass analysis (see aforementioned), P[6] antigen band migrated at a somewhat higher molecular weight on SDS-PAGE gels as compared to P[4] and P[8] (which were at similar mass level, Fig. 3c).

From HIC analysis (Fig. 3d), all 3 antigens appeared heterogeneous when eluted from the phenyl column with the major species accounting for >92% for each protein. Of the 3 antigens, P[4] was most homogeneous at 98.3 ± 0.3% followed by P[8] at 92.8 ± 0.4% and P[6] at 92.3 ± 0.3% ($n = 3$). P[6] was most hydrophobic of the 3 antigens as it eluted at a relatively later retention time as compared to P[4] or P[8] (Fig. 3d). Similarly, through reversed-phase high pressure chromatography analysis (RP-HPLC), the major peak accounted for >93% of each protein. Of the 3 antigens, P[4] was most homogeneous at ~100 ± 0% followed by P[6] at 96.5 ± 0.2% and P[8] at 93.4 ± 0.1% ($n = 3$). P[6] eluted later than P[4] or P[8] as shown in Figure 3e. These RP-HPLC results are consistent with the HIC results (Fig. 3d). No difference in the total area was observed with and without the column in HIC and RP-HPLC assays indicating excellent recovery (i.e., no notable levels of protein were lost because of column adsorption).

Physical Stability Profiles and Comparisons of the Three NRRV Antigens as a Function of Temperature and pH

The HOS and conformational stability of each NRRV antigen was measured and compared as a function of temperature (10°C-90°C) in the formulation buffer. Secondary and tertiary structure stability was evaluated by monitoring CD molar ellipticity at 216 nm and intrinsic Trp fluorescence emission peak intensity, respectively. As shown in Figures 4a and 4b, a single transition event was noted for each antigen and P[8] showed highest onset (T_{onset}) and apparent melting temperature (T_m) as shown in the bar graphs on right. This result suggests that the HOS of the P[8] antigen is the most stable of the 3 antigens against thermal stress. Similar rank order of conformational stability was observed between the 3 antigens with P[8] being most stable (and P[4] was slightly more stable than P[6]) as measured by differential scanning calorimetry and DSF (Figs. 4c and 4d), respectively.

Two light scattering methods (SLS and OD_{350}) were used to assess thermally induced aggregation. Results indicate P[8] is most stable (highest T_{onset} value) as shown in the bar graphs on right panels of Figures 4e and 4f. The P[4] and P[6] antigens showed similar thermal induced aggregation profiles. It is interesting to note the substantially lower T_{onset} values (by ~20°C) by SLS as compared to OD_{350} method for each of the 3 antigens. These differences in SLS versus OD_{350} results likely reflects the higher sensitivity of SLS toward formation of smaller aggregates compared to OD_{350} method which is likely more sensitive to the formation of larger aggregates/particles in solution.

Physical stability of each antigen as a function of both solution pH (from 3.0 to 8.0) and temperature (from 10°C to 90°C) was then monitored to measure changes in secondary structure, tertiary structure, and aggregation behavior. Overall, a pH-dependent destabilization was observed in secondary structure for each antigen (Supplemental Figs. S2a–S2c). For tertiary structure analysis, intrinsic Trp fluorescence mean spectral center of mass peak position showed some subtle changes in the thermal melt profiles, but in general, was not sensitive enough to monitor any potential differences between the antigens (Supplemental Figs. S2d–S2i). By contrast, DSF showed a clear pH-dependent destabilization with
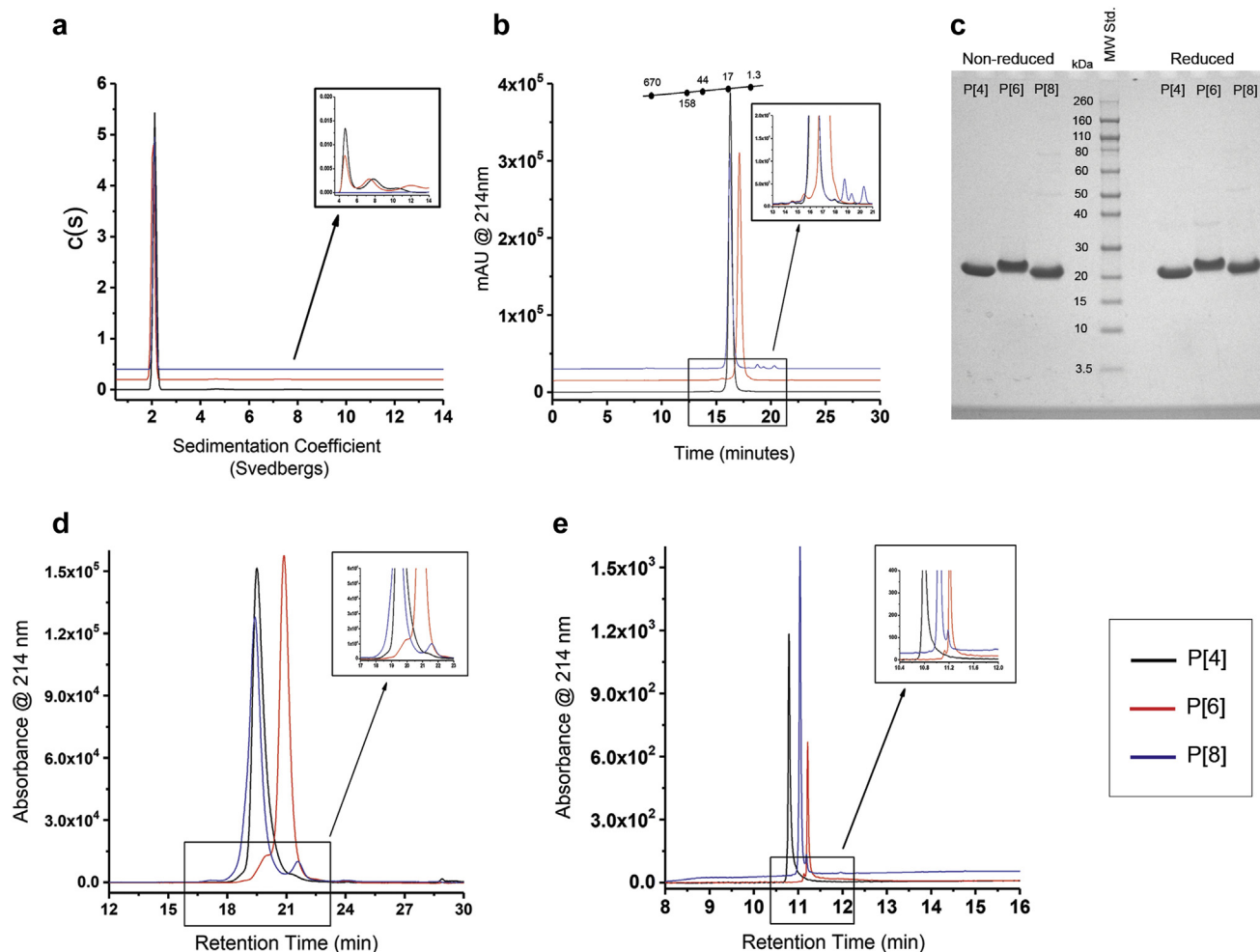
Figure 3. Size, aggregation, and heterogeneity analysis of each of the 3 NRRV antigens in 10 mM PBS, pH 7.2. (a) Representative SV-AUC sedimentation coefficient distribution profiles from 0 to 14 Svedbergs, inset shows c(s) distribution from 4 to 14 Svedbergs for better visualization of aggregate species peak(s). (b) Representative SE-HPLC chromatograms for 3 antigens with inset showing the peaks corresponding to fragments and aggregate species. (c) SDS-PAGE analysis under nonreducing and reducing (+DTT) conditions. (d) Representative HIC chromatograms and (e) representative RP-HPLC chromatograms of the 3 antigens overlay with inset showing the minor peaks for better visualization. DTT, dithiothreitol; SV-AUC, sedimentation velocity analytical ultracentrifugation.

lower pH being less stable as the temperature was increased (Supplemental Figs. S2j–S2l). Aggregation propensity versus solution pH was assessed by monitoring the intensity of total scattered light at 295 nm at 90°. P[8] showed highest intensity values at pH 6.0 and pH 7.0 before precipitation occurred (Supplemental Fig. 2o). In summary, all 3 antigens showed a pH-dependent destabilization at lower pH values (with P[6] being least stable at pH 4.0 and pH 5.0).

To better visualize and compare the entire biophysical stability data sets of each antigen as a function of pH and temperature, a radar chart, data visualization analysis was utilized (Fig. 5).[32] Each radar chart has 5 axes corresponding to the 5 biophysical measurements and the data are mapped to a pentagon such that smaller area of polygon indicate native-like state of protein and relatively larger area represents structural alterations. For each antigen, 4 distinct regions were observed (regions I, II, III/IV, V). Region I corresponds to a native-like structure of the antigen, region II represents partially structurally altered state, region III denotes low pH structurally altered state, region IV shows an aggregation prone region identified specifically for P[8] antigen, and region V represents more extensively aggregated and structurally altered state. Data for each technique can be read in the radar charts by following a particular axis. For instance, SLS signal is mapped to axis "a" (Fig. 5, radar chart key) and if we follow axis "a"

for P[8] antigen in radar charts I to V; I—low signal indicate native-like or monomeric state, II—low to medium signal indicate low levels of aggregation, IV—high signal that is significant aggregation, V—low signal due to precipitation of aggregated protein. If the total relative area of native-like state (i.e., region I) of each antigen is compared; P[8] was most stable with an area of 39%, followed by P[4] with 33%, and P[6] was least stable (27%). In addition, a specific aggregation prone region (region IV) was identified for P[8], suggesting it might be prone to aggregation in that range of pH and temperature (note that P[4] and P[6] are also structurally altered and aggregated in region IV).

Chemical Stability Profiles and Comparisons of the Three NRRV Antigens

After subjecting the 3 NRRV antigens to elevated pH and temperature stress (pH 9.0, 25°C for 6 days), an increasing trend in molecular mass was observed for each protein by intact mass analysis compared to pH 7.2, 4°C control samples (Fig. 6a). Peptide mapping analysis was conducted to further probe the nature of the mass increase. Representative data for P[4] are shown in Figure 6b and similar data for P[6] and P[8] antigens are shown in Supplemental Figures 3a and 3b, respectively. Under no stress
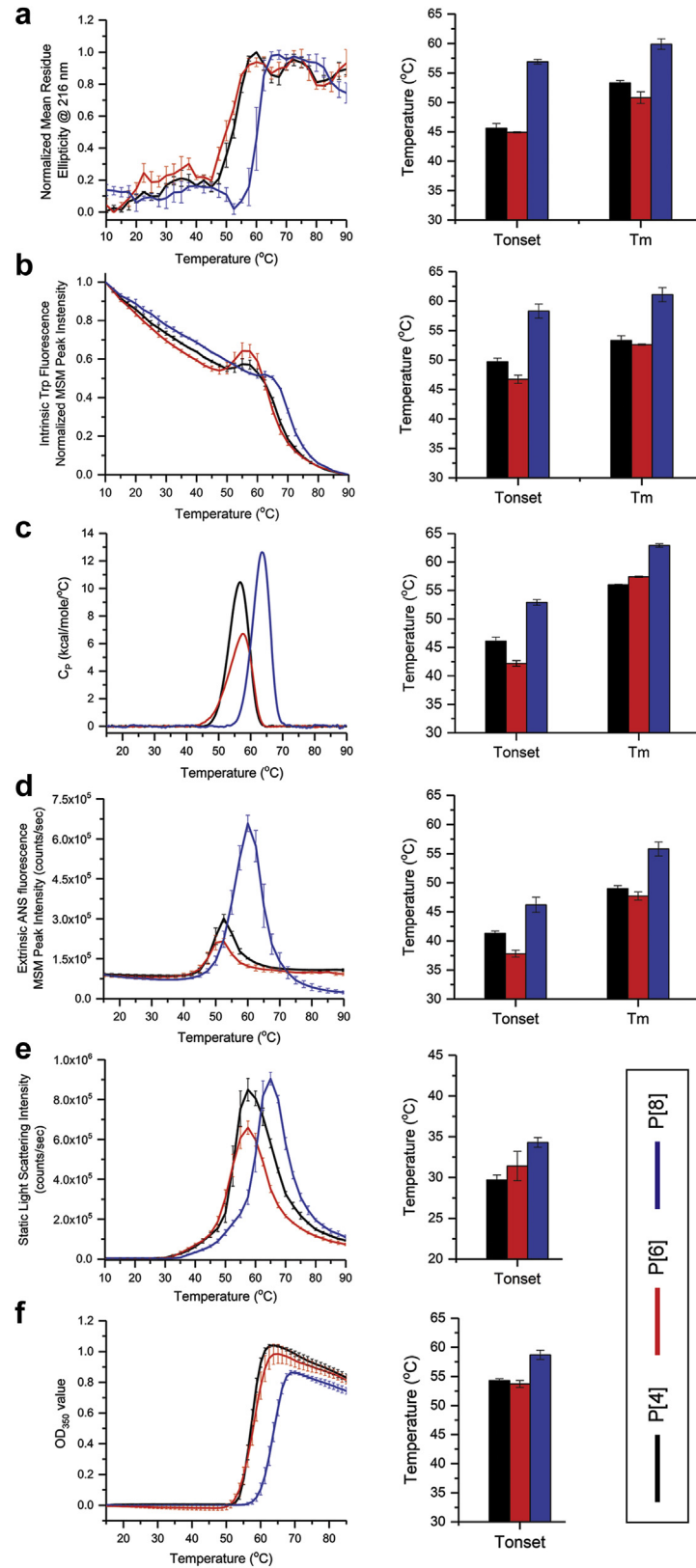
Figure 4. Higher-order structure (HOS) stability and aggregation propensity of the NRRV antigens in 10 mM PBS, pH 7.2, as a function of thermal stress (10°C-90°C). (a) Far-UV CD normalized mean residue ellipticity at 216 nm, (b) intrinsic tryptophan fluorescence normalized MSM peak intensity, (c) representative DSC thermograms of each antigen, (d) extrinsic ANS fluorescence MSM peak intensity, (e) static light scattering intensity at 295 nm, and (f) OD_{350} values for P[4] (black), P[6] (red), and P[8] (blue) antigens. Bar graphs on the right side of each panel show thermal onset (T_{onset}) and thermal melting temperature (T_m) values for each antigen. Error bars represent 1SD from triplicate measurements. DSC, differential scanning calorimetry; MSM, mean spectral center of mass.
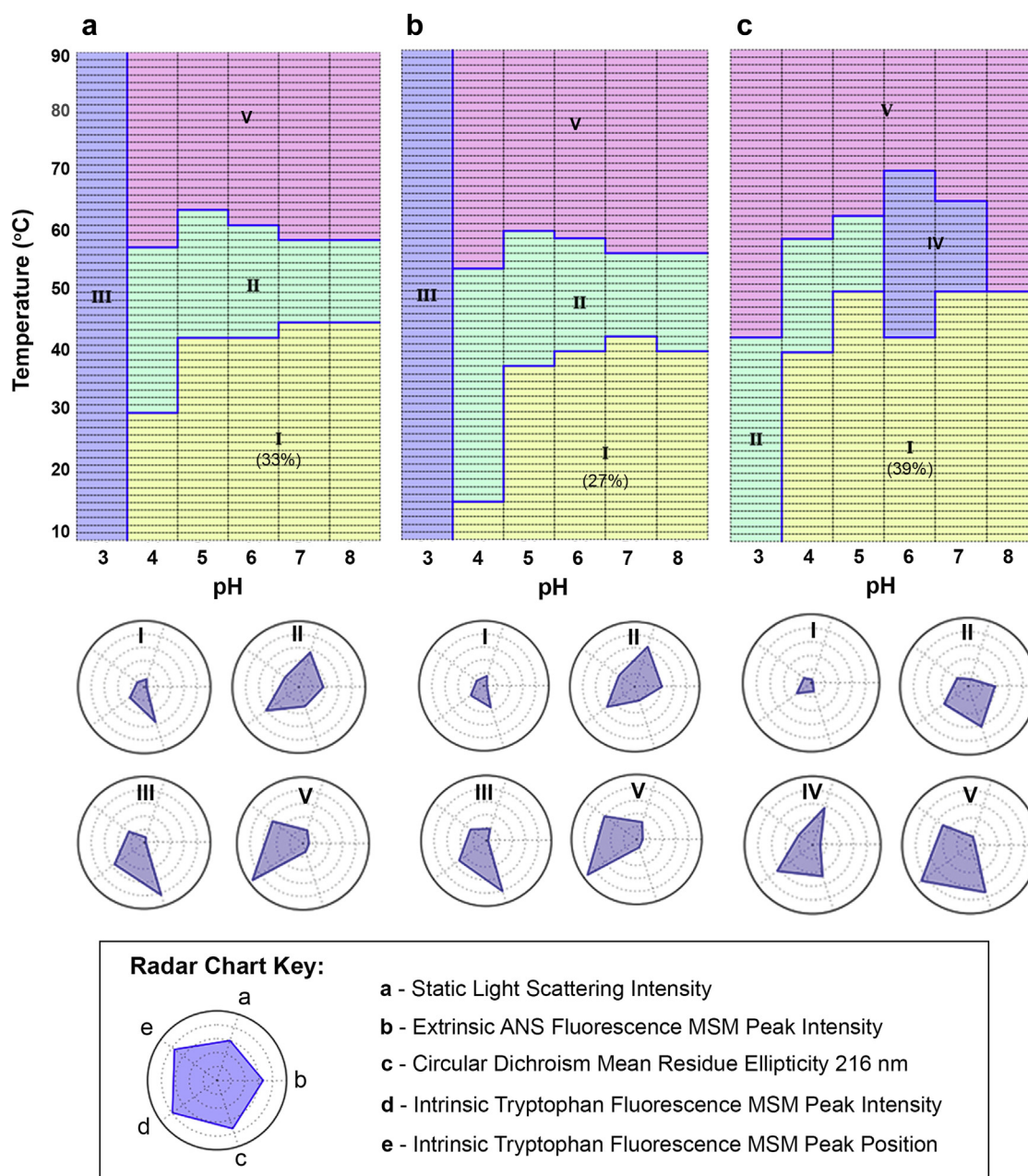
Figure 5. Biophysical stability profile from radar chart analysis of each NRRV antigen versus temperature across the pH range of 3.0 to 8.0. Sample buffer is 20 mM citrate phosphate buffer containing 150 mM NaCl at indicated pH value. (a) P[4], (b) P[6], and (c) P[8] show radar charts generated from multivariate stability data sets shown in Supplemental Figure S2. Radar chart key is provided in the bottom panel (see text for further explanation).

conditions (pH 7.2, 4°C), deamidation was observed at Asn[7] in each antigen and at each of the Asn-Gly (NG) sites (P[4] and P[8] antigens have 2 NG sites, whereas, P[6] has none). On incubation at pH 9.0 25°C for 6 days, P[4] antigen showed increased levels of deamidation at Asn[7] and Asn-Gly residues (Asn[47] and Asn[179]) as shown in Figure 6c. For P[6] antigen, Asn[7] showed increased levels of deamidation under the same stress conditions. The P[8] antigen also showed increased levels of Asn[7] deamidation and an increasing trend of deamidation was observed for the Asn-Gly residues (Asn[46] and Asn[178]) under similar stress, although it was not statistically significant under these conditions (more notable levels of Asn[46] and Asn[178] deamidation were observed in P[8] when subjected to more aggressive stress condition of pH 9.0 40°C for 6 days; however, P[4] and P[6] antigens could not be tested for deamidation

under this condition due to aggregation; data not shown. Overall, forced deamidation studies demonstrated the susceptibility of Asn[7], Asn[47], and Asn[179] in P[4], Asn[7] in P[6], and Asn[7], Asn[46], and Asn[178] in P[8] toward deamidation under basic conditions at elevated temperature with the Asn[7] residue being the most labile across all 3 antigens.

SDS-PAGE analysis (under non-reducing conditions) of the same elevated pH and temperature stressed P[6] samples showed an additional band corresponding to dimeric species which was absent or less abundant under reducing condition as shown in Figure 7a. This result suggests the dimeric species were linked with intermolecular disulfide bond because each NRRV antigen has single Cys residue. A faint dimeric band was also present under non-reducing condition for P[6] pH 9.0, 4°C stressed samples. RP
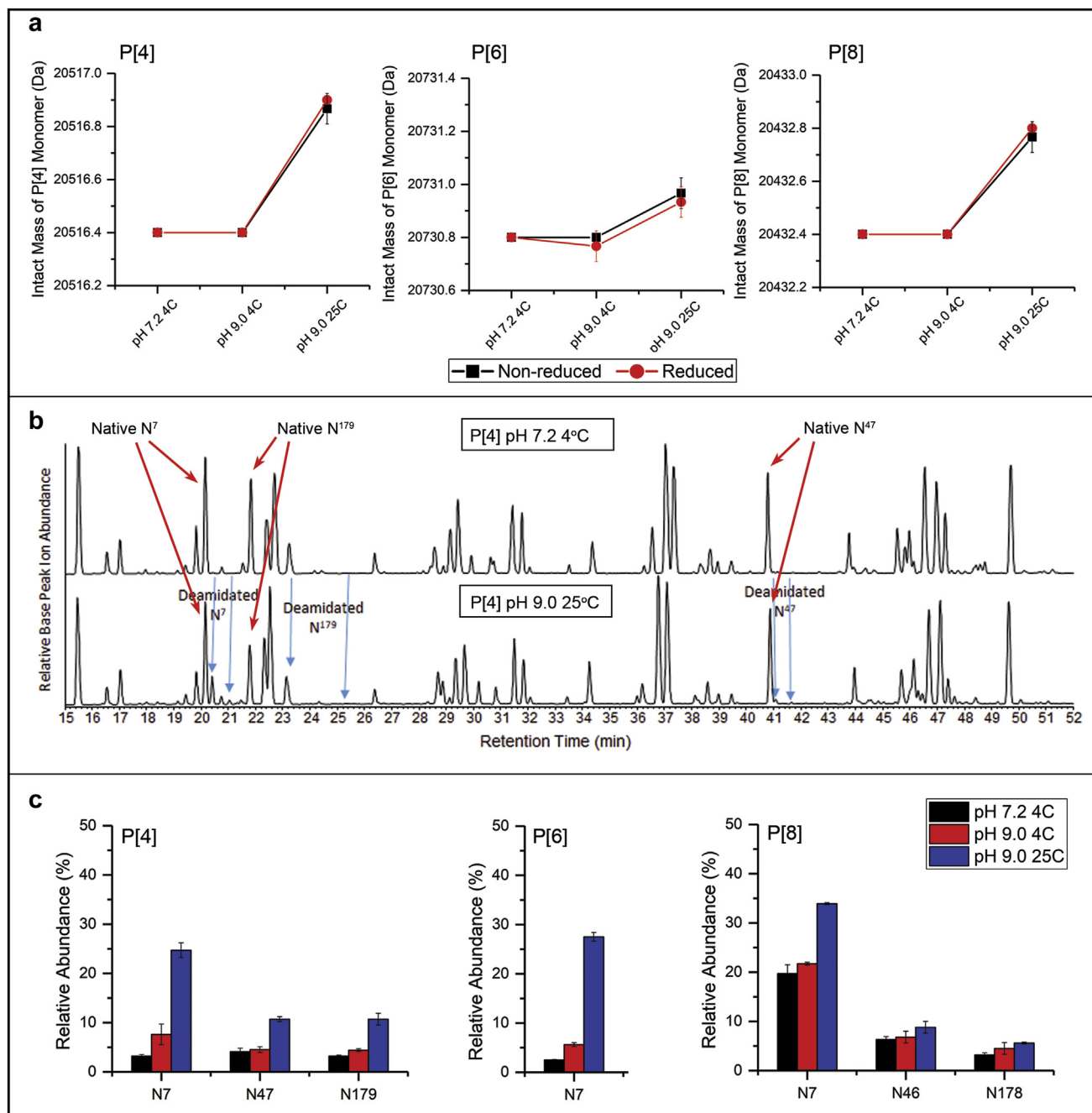
Figure 6. Forced degradation (Asn deamidation) studies of each NRRV antigen after incubation at pH 9.0 25°C for 6 d. (a) Monomer species mass from intact mass analysis of reduced (red) and nonreduced (black) samples for each antigen. (b) Representative total ion chromatogram from peptide map analysis of reduced, alkylated, and chymotrypsin digested P[4] samples, pH 7.2 4°C (top) and pH 9.0 25°C (bottom), native Asn peaks are pointed by red arrows and deamidated Asn peaks are pointed out by blue arrows (see Supplemental Fig. S3 for peptide map data with P[6] and P[8] antigens). (c) Percentage deamidation of different Asn residues in each antigen obtained from the peptide mapping analysis under reducing conditions. Error bars represent 1SD from triplicate vials.

ultra-high pressure chromatography analysis showed an additional peak (~34.5 min) eluting at later retention time than the monomer peak (~30 min) as shown in Figure 7c. This additional peak was identified as P[6] dimer species by MS^1 analysis (right panel, Fig. 7c) which correlates with SDS-PAGE results. However, the dimeric species were not observed by intact mass analysis presumably due to their low abundance and a single peak corresponding to monomeric protein was observed in control and stressed samples (Fig. 7b). For the P[4] antigen, a very faint HMW smear was observed at pH 9.0, 25°C (but not at pH 9.0, 4°C) under non-reducing conditions in SDS-PAGE analysis as shown in Supplemental Figure S4a. The P[4] dimer species also eluted at later retention time on reversed-phase chromatography as confirmed by the MS^1 analysis of the eluting peaks (see Supplemental Fig. S4c). For the P[8] antigen, no additional HMW species was observed under the tested conditions suggesting higher stability of this antigen to non-native disulfide formation as compared to P[4] and P[6] (see Supplemental Fig. S5). Overall, the chemical stability profile demonstrates that P[6] is more susceptible to this non-native disulfide bond reaction compared to P[4] and P[8] antigens.
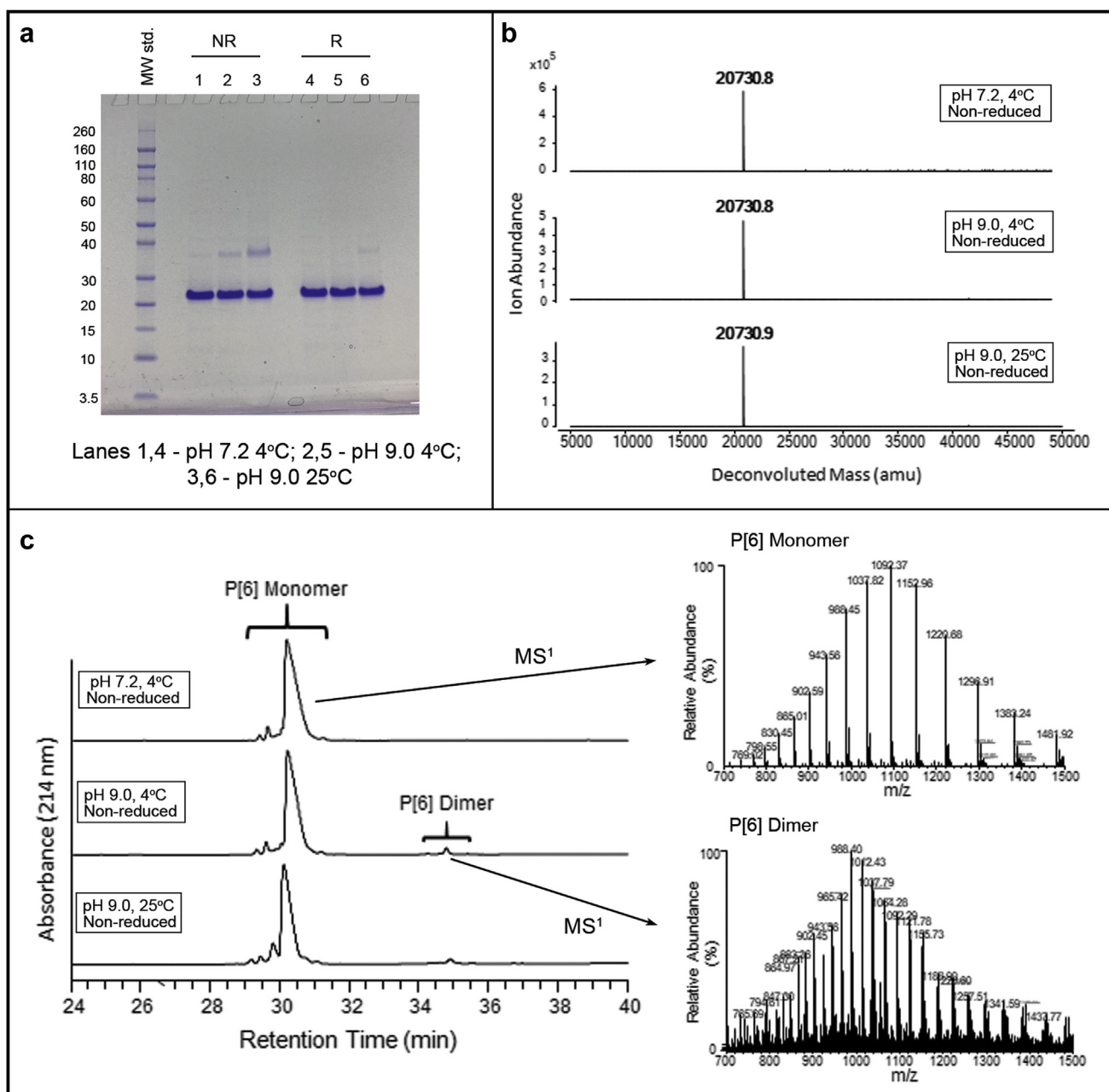
Figure 7. Forced degradation (non-native disulfide formation) studies with P[6] antigen after incubation at pH 9.0 25°C for 6 d (a) SDS-PAGE analysis, (b) intact mass analysis, and (c) RP-UHPLC analysis of the stressed and control samples, further, MS[1] spectra confirming the molecular masses of the eluting peaks to the P[6] monomer and dimer species are shown. Refer to Supplemental Figures S4 and S5 for similar data with P[4] and P[8] antigens, respectively. RP-UHPLC, RP ultra-high pressure chromatography.

In terms of oxidative stress reactions, the 3 NRRV antigens were subjected to different amounts of H_2O_2. Figures 8a and 8b show representative data for P[6] antigen, a prominent peak for native species and low level of oxidized species were observed in the control sample (without H_2O_2) as measured by intact mass spectrometry and LC-MS peptide mapping, respectively. With the increasing amount of H_2O_2 the relative abundance of native species decreased, and the number and abundance of oxidized species increased. Peptide mapping analysis was conducted to identify the amino acids undergoing oxidation and also to quantify the oxidation relative to the control sample. As shown in Figure 8c, for P[6] antigen which has 2 Met residues, Met[1] was most susceptible to oxidation followed by Met[100]. Similar observations were made for the 2 Met residues in P[8] antigen (Met[1] more susceptible than

Met[99]), as shown in Figure 8c and Supplemental Figure S8. The P[4] antigen has 3 Met residues and their susceptibility to oxidation can be rank ordered as Met[1] > Met[100] > Met[124] (Fig. 8c). Oxidized Met[100] in P[4], P[6], and Met[99] in P[8] were only detectable when samples were incubated with ≥0.1% H_2O_2 (≥1000 ppm) as described in Figure 8c. Similarly, Met[124] in P[4] was oxidized only when exposed to ≥0.25% H_2O_2 (data not shown). No detectable change in the elution profile of digested peptides was observed until exposure to 0.1% H_2O_2, at which point the elution profile was altered and sequence coverage was reduced from 100% to ~80% for all 3 antigens (Supplemental Figs. S6-S8). In addition, the elution profiles of each sample (stressed or control) of a particular antigen were similar on a reversed-phase column, in which the primary peak eluted at ~9.5 min (P[4]), ~9.7 min (P[6]), and ~9.5 min (P[8])
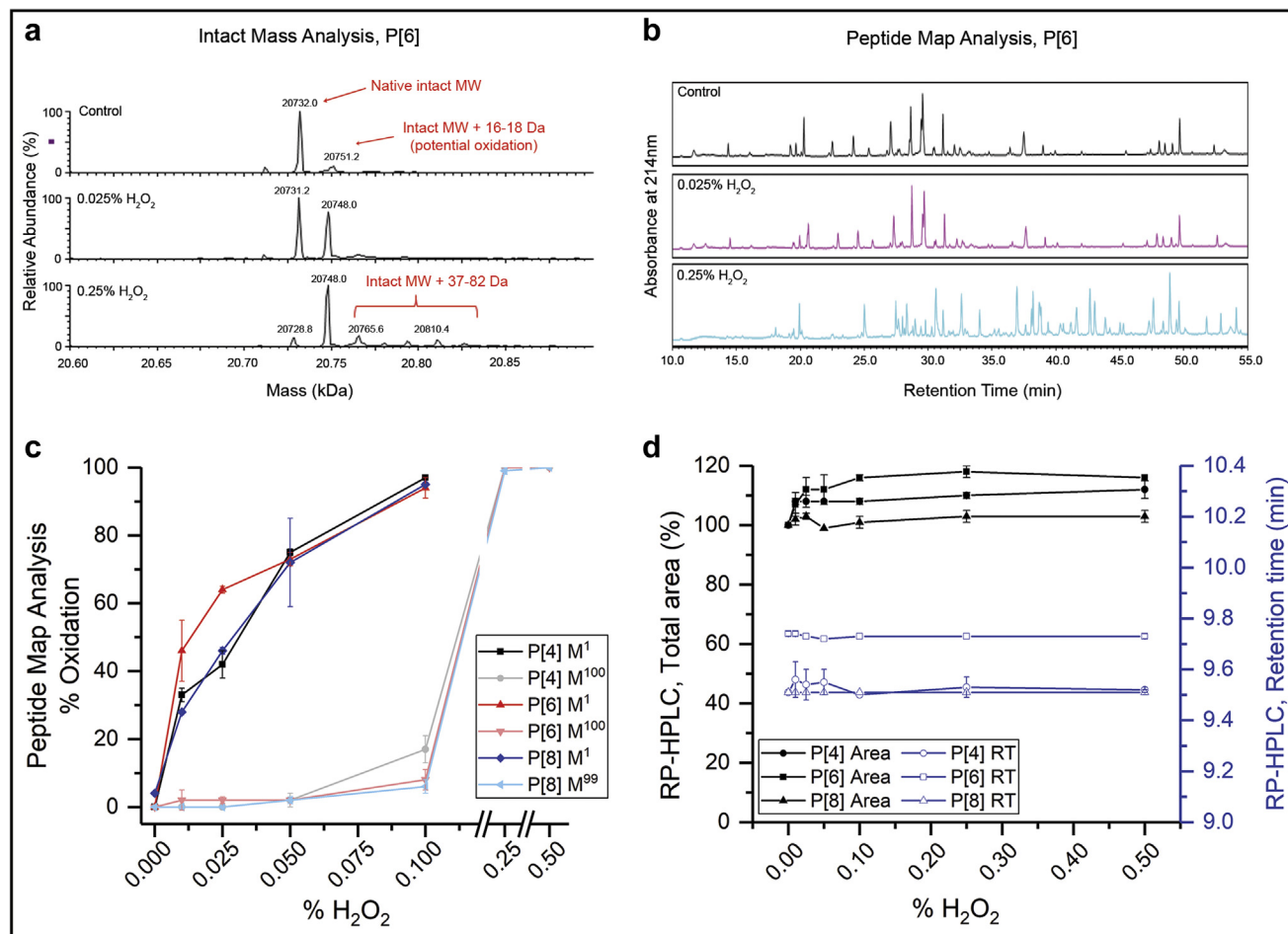
Figure 8. Forced oxidation studies with NRRV antigens as a function of hydrogen peroxide concentration. Representative (a) deconvoluted mass spectra for intact mass analysis, and (b) peptide map analysis of P[6] antigen under reducing (+DTT) condition. See Supplemental Figures S6-S8 for the complete data sets of the 3 antigens. (c) Hydrogen peroxide effect on the relative percent oxidation of 2 of 2 methionine residues for P[6], P[8], and 2 of 3 methionine residues for P[4]. (d) % total area and retention time of main peak in RP-HPLC chromatograms of each antigen, see Supplemental Figure S9 for individual chromatograms. Error bars represent 1SD from triplicate measurements.

as shown in Figure 8d and Supplemental Figure S9. In addition, the area of the peak corresponding to native species did not change substantially between samples (Fig. 8d) indicating no measurable loss of protein. In summary, intact protein mass measurement and peptide mapping by LC-MS methods are assays of choice to detect and monitor oxidation. The Met[1] residue in each NRRV protein antigen was most susceptible to H_2O_2—induced oxidation, and oxidation was also observed at other Met residues under more aggressive stress conditions ($\geq$1000 ppm H_2O_2).

Structural Modeling and Comparisons of the Three NRRV Antigens

As a first step to facilitate the analysis of the physicochemical data generated in this work, a schematic is provided in Figure 9a which describes the composition and nomenclature of the 3 NRRV antigens studied in this work (refer to Introduction section for more details). The X-ray crystal structures for VP8-P[4] (i.e., ΔVP8* from DS-1 (G2P[4]) strain) and VP8-P[8] (i.e., ΔVP8* from Wa (G1P[8]) strain) have been determined. These proteins bind to carbohydrates on target epithelial cell receptors and are involved in host cell recognition and attachment during RV infection.[30,31] We used I-TASSER modeling to model the 3D structure of the complete NRRV antigen, that is including the P2 epitope, by using the available crystal structures of the ΔVP8* protein from DS-1 and Wa strains of human RV as template. As described in the methods

section, I-TASSER modeling predicted 5 structures with the lowest energy state for each antigen and the major difference between the 5 predicted structures is the unstructured or random orientation of the P2 epitope indicating its flexible nature. Figure 9b shows the predicted 3D structure of each NRRV antigen including the 3 key structural elements: the P2 epitope (black), GSGSG linker (cyan), and ΔVP8* protein (gray). The chemically labile residues or "weak spots" identified for each antigen in this work are highlighted on the structural models (Met—magenta, Asn—green, Cys—red) in Figure 9b.

Discussion

In this work, the primary and higher-order structures, post-translational modifications, and product-based impurities (e.g., charge heterogeneity, aggregates) of the 3 recombinant NRRV protein antigens were measured and compared using a wide variety of physicochemical characterization tools. In addition, degradation pathways of each of these proteins were elucidated via forced degradation studies to identify "weak spots" in terms of physical and chemical stability profiles. Although the potential impact of physicochemical structural alterations on immunogenicity is unknown at this time, developing such stability-indicating analytical tools and applying the structural knowledge gained in this work will be useful to (1) set critical manufacturing process parameters to ensure
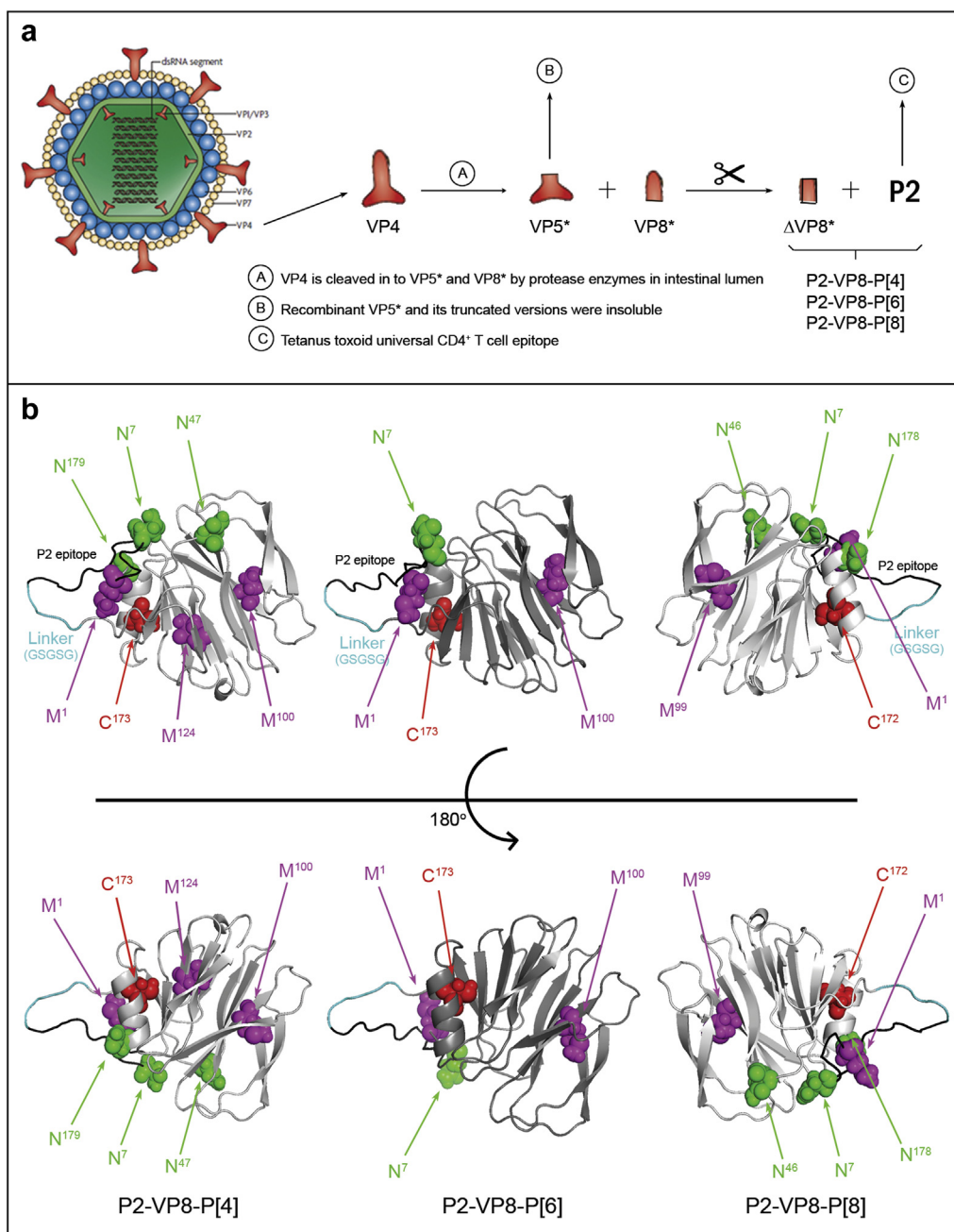
Figure 9. Structural modeling of the 3 NRRV protein antigens. (a) Schematic description of the protein composition and nomenclature of each NRRV antigen, and (b) 3D structure prediction of each NRRV antigen using I-TASSER modeling; ΔVP8* protein is shown in gray, GSGSG linker in cyan, and P2 epitope in black. Residues susceptible to chemical degradation under stressed conditions are highlighted (Cys—red, Asn—green, Met—magenta).

consistency, (2) monitor key structural attributes during comparability assessments, and (3) develop stable formulations for the bulk drug substance and adjuvanted final drug product. The pharmaceutical stability profiles encountered during manufacturing and storage are not only dependent on such intrinsic properties (e.g., primary sequence/post-translational modifications,[33] conformational stability,[34] solubility[35]), but also extrinsic stress factors (e.g., storage temperature, freeze-thaw, agitation).[36,37]

Primary Structure, Post-Translational Modifications, and Chemical Stability Profile

An additional Met residue identified at N-terminus of each antigen was not unexpected because these antigens were expressed in *E. coli* and the efficiency of methionine aminopeptidase, enzyme responsible for excision of N-terminal methionine during translation, is about 30%-60% depending on the host.[38] Residue next to the N-terminal Met for each NRRV antigen is Glu with a bulky side chain which could also hinder the efficiency of methionine aminopeptidase by steric effects as noted in the literature.[39,40] Peptides generated after chymotrypsin digestion during peptide mapping analysis of each antigen showed distinct and very reproducible elution profile on a RP column which could be used as an identity test during future development of these antigens.

Oxidation via reactive oxygen species is a commonly observed chemical degradation pathway for protein biotherapeutics and vaccine antigens which can affect product quality, stability, and raises immunogenicity concerns.[41,42] Peroxides are an example of

reactive oxygen species which can come in contact with vaccine drug products through various means such as the use of vaporized H_2O_2 as a sterilizing agent, as contaminants in formulation excipients such as polysorbates, and potentially even as trace quantities present in water depending on its source.[43-46] Under forced degradation conditions (100-5000 ppm H_2O_2), the Met[1] residue was most sensitive to oxidation in each of the 3 NRRV antigens. Interestingly, the Met[100] or Met[99] residue in each antigen, and Met[124] in P[4] antigen were less prone to H_2O_2-induced oxidation compared to Met[1] (which could be due to their reduced solvent accessibility within the three dimensional (3D) structure of the protein; see below).

Forced deamidation studies confirmed that Asn[7] in each NRRV antigen is susceptible to deamidation under conditions of basic pH and elevated temperature. Asn[7] in these proteins is followed by Ser residue which is the second most susceptible sequence for deamidation after NG sequence.[36] The P[4] and P[8] antigens each have 2 NG sites (P[6] has none) in their primary sequence, and the Asn residues at these sites also showed increasing trend in deamidation levels for stressed samples (Fig. 7c). It is known that Asn deamidation in proteins and peptides depends on a combination of factors including their primary sequence, 3D structure (i.e., flexibility and solvent accessibility of these sites) and solution conditions (i.e., pH, buffer type, temperature).[47,48] Overall, the peptide mapping method was able to detect and quantify the Asn deamidation in each NRRV antigen and thus will be a valuable tool during future formulation development and analytical comparability assessments.

The labile Met[1] and Asn[7] residues are both located in the P2 epitope region of these antigens which is highly flexible and unstructured as predicted by I-TASSER modeling (Fig. 9b) and some preliminary hydrogen deuterium exchange mass spectrometry studies (data not shown). Higher flexibility of this P2 region would explain the higher propensity of Met[1] to oxidation and Asn[7] to deamidation due to their relatively higher solvent accessibility compared to other Met and Asn residues which could be buried inside the protein structure.

In addition, the 1 free Cys residue in each NRRV antigen is also a "weak spot" in each antigen. Under stressed conditions of elevated pH and temperature, we observed reducible dimeric or multimeric species which were linked with intermolecular disulfide bonds. The P[6] antigen showed the highest susceptibility to this degradative reaction, followed by P[4], whereas dimeric or multimeric species were not observed for P[8] under the tested conditions. This result is in agreement with the physical stability data which showed higher conformational stability of P[8] antigen suggesting some sort of conformational alteration is needed for the Cys residue to get more solvent exposed allowing it to form non-native intermolecular disulfide bonds. Susceptibility of Cys[173] in P[4] and P[6] to non-native disulfide formation could be due to lower conformational stability of the helical domain containing this Cys residue, thus exposing the free Cys to solvent and promoting the degradative reaction. Although the P[8] antigen was more stable to this degradative reaction under these conditions, disulfide linked covalent aggregates were formed with all 3 NRRV antigens when subjected to agitation stress (see companion paper by Agarwal et al.[27]).

Size, Higher-Order Structure, and Physical Stability Profile

Each antigen was primarily monomeric in size and P[6] eluted at later retention times on a size-exclusion chromatography column compared to P[4] and P[8]. The smaller overall size of P[6] was in agreement with the sedimentation coefficient values. These results are consistent with P[6] being more globular or compact in its overall conformation. In addition, GRAVY analysis indicated P[6] is most hydrophobic of the 3 antigens with a GRAVY score of −0.466, as compared to P[4] and P[8] with scores of −0.573 and −0.569, respectively. This could also explain in part its relatively more compact 3D structure. The more hydrophobic nature of P[6] was also confirmed by the observed longer retention times on HIC and RP columns to P[4] and P[8].

The HOS of each NRRV antigen was primarily β-sheet in composition as suggested by available crystallographic information on ΔVP8* (PDB ID: 2AEN, 2DWR) and predicted by I-TASSER modeling (Fig. 9b). The FTIR and far-UV CD spectroscopic results in this work are consistent with this secondary structure composition. Some minor differences in environment around Trp residues were observed between the 3 antigens; the average Trp residues appeared to be more buried for P[4] and P[6] antigens compared to P[8].

Differences in structural integrity and physical stability of the 3 NRRV antigens (with 66%-80% sequence homology) highlight the importance of differences in the primary and HOS structures of otherwise "similar" antigens that can govern their pharmaceutical stability profiles and developability as a vaccine candidate. Solution pH plays an important in controlling the ionization state of different residues which keep the molecule in its marginally stable HOS, native conformation.[49,50] Each NRRV antigen underwent structural alterations at pH 3.0. The P[6] antigen was least stable at pH 4.0 and 5.0 followed by P[4] and P[8]. Radar chart analysis is a data visualization tool that has been used to summarize and compare large biophysical data sets to study the effect of various stresses (e.g., pH, temperature) on physical stability of a wide variety of macromolecules including vaccine and protein drug candidates.[34,51-57] Radar chart analysis in this work showed the structural integrity and conformational stability of 3 NRRV antigens as a function of pH and temperature. P[8] was the most stable, followed by P[4], and P[6] was least stable. In addition, non-native dimer formation was observed for P[6] and P[4] antigens, no dimeric species was recorded for P[8]. Interestingly, the P[8] antigen showed relatively lowest stability against shaking (i.e., colloidal stability) and freeze-thaw stresses resulting in the highest levels of particle formation when comparing the 3 NRRV antigens (see companion paper, Agarwal et al.[27]).

Ongoing and Future Work

In terms of ongoing and future work, both physical and chemical degradation processes elucidated in this work (leading to structural alterations, chemical changes, or aggregate formation) could be detrimental to the development of NRRV antigens as a candidate vaccine without appropriate formulation development. The physicochemical characterization tools developed in this work were applied to monitor and characterize protein aggregation and particle formation during agitation and freeze-thaw stresses, and to develop candidate formulations to minimize their occurrence during storage and processing of these NRRV antigens as frozen liquid bulk drug substances (see companion paper, Agarwal et al.[27]). It is important to note that these assays can also be adopted and modified to characterize and assess the physicochemical stability of the final vaccine drug product (a trivalent mixture of the 3 NRRV antigens formulated with an aluminum adjuvant) during storage as well as any potential effects of chemical alterations of the NRRV antigens on their interaction with aluminum adjuvants (work in progress). However, it is essential as part of future work to better correlate these physicochemical changes with *in vitro* potency using immunochemical (binding) assays (e.g., ELISA, biolayer interferometry, or surface plasmon resonance) utilizing antibody reagents which are specific to each antigen and bind to neutralizing

epitope(s). Eventually the results from physicochemical and *in vitro* potency assays need to be correlated with *in vivo* immunogenicity (animal studies) to determine their true impact on biological potency of the vaccine. For example, the chemical variants of NRRV antigens generated during forced degradation studies (e.g., oxidation, deamidation, and intermolecular disulfide bond formation) may or may not form during real-time storage, and similarly, may or may not impact their antigenicity and immunogenicity. Finally, the physicochemical analytical tools described in this work can be used during future comparability assessments of different lots of each of the NRRV antigens made from scaled-up manufacturing processes. It is not uncommon to introduce changes in the manufacturing processes during scale-up or switching to a different manufacturing site to keep the cost of vaccine production low, which is a key focus for the success of this subunit RV vaccine candidate for use in the developing world.

Acknowledgments

References

1. Tate JE, Burton AH, Boschi-Pinto C, Parashar UD, World Health Organization-Coordinated Global Rotavirus Surveillance Network. Global, regional, and national estimates of rotavirus mortality in children <5 years of age, 2000-2013. *Clin Infect Dis*. 2016;62(Suppl 2):S96-S105.
2. Parashar UD, Hummelman EG, Bresee JS, Miller MA, Glass RI. Global illness and deaths caused by rotavirus disease in children. *Emerg Infect Dis*. 2003;9(5):566-572.
3. Wang CM, Chen SC, Chen KT. Current status of rotavirus vaccines. *World J Pediatr*. 2015;11(4):300-308.
4. Chandran A, Fitzwater S, Zhen A, Santosham M. Prevention of rotavirus gastroenteritis in infants and children—rotavirus vaccine safety, efficacy, and potential impact of vaccines. *Biologics*. 2010;4:213-229.
5. Burnett E, Parashar U, Tate J. Rotavirus vaccines: effectiveness, safety, and future directions. *Paediatr Drugs*. 2018;20(3):223-233.
6. O'Ryan M. Rotavirus vaccines: a story of success with challenges ahead. *F1000Res*. 2017;6:1517.
7. Jonesteller CL, Burnett E, Yen C, Tate JE, Parashar UD. Effectiveness of rotavirus vaccination: a systematic review of the first decade of global postlicensure data, 2006-2016. *Clin Infect Dis*. 2017;65(5):840-850.
8. Keith Grimwood SBL, Richard J, Milne. Rotavirus infections and vaccines-burden of illness and potential impact of vaccination. *Pediatr Drugs*. 2010;12(4):235-256.
9. Tate JE, Parashar UD. Rotavirus vaccines in routine use. *Clin Infect Dis*. 2014;59(9):1291-1301.
10. Desselberger U. Differences of rotavirus vaccine effectiveness by Country: likely causes and contributing factors. *Pathogens*. 2017;6(4). Article number 65.
11. Lazarus RP, John J, Shanmugasundaram E, et al. The effect of probiotics and zinc supplementation on the immune response to oral rotavirus vaccine: a randomized, factorial, design, placebo-controlled study among Indian infants. *Vaccine*. 2018;36(2):273-279.
12. Parker EPK, Praharaj I, Zekavati A, et al. Influence of the intestinal microbiota on the immunogenicity of oral rotavirus vaccine given to infants in south India. *Vaccine*. 2018;36(2):264-272.
13. Jiang V, Jiang B, Tate J, Parashar UD, Patel MM. Performance of rotavirus vaccines in developed and developing countries. *Hum Vaccines*. 2010;6(7):532-542.
14. Pasetti MF, Simon JK, Sztein MB, Levine MM. Immunology of gut mucosal vaccines. *Immunol Rev*. 2011;239(1):125-148.
15. Jiang B, Gentsch JR, Glass RI. Inactivated rotavirus vaccines: a priority for accelerated vaccine development. *Vaccine*. 2008;26(52):6754-6758.
16. Groome MJ, Koen A, Fix A, et al. Safety and immunogenicity of a parenteral P2-VP8-P[8] subunit rotavirus vaccine in toddlers and infants in South Africa: a randomised, double-blind, placebo-controlled trial. *Lancet Infect Dis*. 2017;17(8):843-853.
17. Fix AD, Harro C, McNeal M, et al. Safety and immunogenicity of a parenterally administered rotavirus VP8 subunit vaccine in healthy adults. *Vaccine*. 2015;33(31):3766-3772.
18. Franco MA, Angel J, Greenberg HB. Immunity and correlates of protection for rotavirus vaccines. *Vaccine*. 2006;24(15):2718-2731.
19. Wen X, Wen K, Cao D, et al. Inclusion of a universal tetanus toxoid CD4(+) T cell epitope P2 significantly enhanced the immunogenicity of recombinant rotavirus DeltaVP8* subunit parenteral vaccines. *Vaccine*. 2014;32(35):4420-4427.
20. Wen X, Cao D, Jones RW, Li J, Szu S, Hoshino Y. Construction and characterization of human rotavirus recombinant VP8* subunit parenteral vaccine candidates. *Vaccine*. 2012;30(43):6121-6126.
21. Hickey JM, Toprani VM, Kaur K, et al. Analytical comparability assessments of 5 recombinant CRM197 proteins from different manufacturers and expression systems. *J Pharm Sci*. 2018;107(7):1806-1819.
22. Federici M, Lubiniecki A, Manikwar P, Volkin DB. Analytical lessons learned from selected therapeutic protein drug comparability studies. *Biologicals*. 2013;41(3):131-147.
23. Lubiniecki A, Volkin DB, Federici M, et al. Comparability assessments of process and product changes made during development of two different monoclonal antibodies. *Biologicals*. 2011;39(1):9-22.
24. Kumru OS, Joshi SB, Smith DE, Middaugh CR, Prusik T, Volkin DB. Vaccine instability in the cold chain: mechanisms, analysis and formulation strategies. *Biologicals*. 2014;42(5):237-259.
25. Volkin DB, Middaugh CR. Vaccines as physically and chemically well-defined pharmaceutical dosage forms. *Expert Rev Vaccines*. 2010;9(7):689-691.
26. Dey AK, Malyala P, Singh M. Physicochemical and functional characterization of vaccine antigens and adjuvants. *Expert Rev Vaccines*. 2014;13(5):671-685.
27. Agarwal S, Sahni N, Hickey JM, et al. Characterizing and minimizing aggregation and particle formation of three recombinant protein vaccine bulk antigens for use in a trivalent rotavirus vaccine candidate. *J Pharm Sci*. 2020;109(1):394-406.
28. Toprani VM, Hickey JM, Sahni N, et al. Structural characterization and physicochemical stability profile of a double mutant heat labile toxin protein based adjuvant. *J Pharm Sci*. 2017;106(12):3474-3485.
29. Toprani VM, Sahni N, Hickey JM, et al. Development of a candidate stabilizing formulation for bulk storage of a double mutant heat labile toxin (dmLT) protein based adjuvant. *Vaccine*. 2017;35(41):5471-5480.
30. Blanchard H, Yu X, Coulson BS, von Itzstein M. Insight into host cell carbohydrate-recognition by human and porcine rotavirus from crystal structures of the virion spike associated carbohydrate-binding domain (VP8*). *J Mol Biol*. 2007;367(4):1215-1226.
31. Monnier N, Higo-Moriguchi K, Sun ZY, Prasad BV, Taniguchi K, Dormitzer PR. High-resolution molecular and antigen structure of the VP8* core of a sialic acid-independent human rotavirus strain. *J Virol*. 2006;80(3):1513-1523.
32. Kim JH, Iyer V, Joshi SB, Volkin DB, Middaugh CR. Improved data visualization techniques for analyzing macromolecule structural changes. *Protein Sci*. 2012;21(10):1540-1553.
33. More AS, Toth RT, Okbazghi SZ, et al. Impact of glycosylation on the local backbone flexibility of well-defined IgG1-Fc glycoforms using hydrogen exchange-mass spectrometry. *J Pharm Sci*. 2018;107(9):2315-2324.
34. More AS, Toprani VM, Okbazghi SZ, et al. Correlating the impact of well-defined oligosaccharide structures on physical stability profiles of IgG1-Fc glycoforms. *J Pharm Sci*. 2016;105(2):588-601.
35. Toprani VM, Joshi SB, Kueltzo LA, Schwartz RM, Middaugh CR, Volkin DB. A micro-polyethylene glycol precipitation assay as a relative solubility screening tool for monoclonal antibody design and formulation development. *J Pharm Sci*. 2016;105(8):2319-2327.
36. Manning MC, Chou DK, Murphy BM, Payne RW, Katayama DS. Stability of protein pharmaceuticals: an update. *Pharm Res*. 2010;27(4):544-575.
37. Zbacnik TJ, Holcomb RE, Katayama DS, et al. Role of buffers in protein formulations. *J Pharm Sci*. 2017;106(3):713-733.
38. Giglione C, Fieulaine S, Meinnel T. N-terminal protein modifications: bringing back into play the ribosome. *Biochimie*. 2015;114:134-146.
39. Hirel PH, Schmitter MJ, Dessen P, Fayat G, Blanquet S. Extent of N-terminal methionine excision from Escherichia coli proteins is governed by the side-chain length of the penultimate amino acid. *Proc Natl Acad Sci U S A*. 1989;86:8247-8251.
40. Vassileva-Atanassova A, Mironova R, Nacheva G, Ivanov I. N-terminal methionine in recombinant proteins expressed in two different Escherichia coli strains. *J Biotechnol*. 1998;69(1):63-67.
41. Li S, Schöneich C, Borchardt RT. Chemical instability of protein pharmaceuticals- mechanisms of oxidation and strategies for stabilization. *Biotechnol Bioeng*. 1995;48:490-500.
42. Torosantucci R, Schoneich C, Jiskoot W. Oxidation of therapeutic proteins and peptides: structural and biological consequences. *Pharm Res*. 2014;31(3):541-553.
43. Cooper WJ, Zika RG. Photochemical formation of hydrogen peroxide in surface and ground waters exposed to sunlight. *Science*. 1983;220(4598):711-712.
44. Cooper WJ, Zika RG, Petasne RG, Plane JM. Photochemical formation of hydrogen peroxide in natural waters exposed to sunlight. *Environ Sci Technol*. 1988;22(10):1156-1160.
45. Ha E, Wang W, Wang YJ. Peroxide formation in polysorbate 80 and protein stability. *J Pharm Sci*. 2002;91(10):2252-2264.
46. Wasylaschuk WR, Harmon PA, Wagner G, et al. Evaluation of hydroperoxides in common pharmaceutical excipients. *J Pharm Sci*. 2007;96(1):106-116.
47. Kosky AA, Razzaq UO, Treuheit MJ, Brems DN. The effects of alpha-helix on the stability of Asn residues: deamidation rates in peptides if varying helicity. *Protein Sci*. 1999;8:2519-2523.

48. Robinson NE, Robinson AB. Molecular clocks. *Proc Natl Acad Sci U S A*. 2001;98(3):944-949.
49. Mason BD, Schoneich C, Kerwin BA. Effect of pH and light on aggregation and conformation of an IgG1 mAb. *Mol Pharm*. 2012;9(4):774-790.
50. Li CH, Narhi LO, Wen J, et al. Effect of pH, temperature, and salt on the stability of Escherichia coli- and Chinese hamster ovary cell-derived IgG1 Fc. *Biochemistry*. 2012;51(50):10056-10065.
51. Qi W, Zeng Y, Orgel S, et al. Preformulation study of highly purified inactivated polio vaccine, serotype 3. *J Pharm Sci*. 2014;103(1):140-151.
52. Kumru OS, Joshi SB, Thapa P, et al. Characterization of an oncolytic herpes simplex virus drug candidate. *J Pharm Sci*. 2015;104(2):485-494.
53. Kissmann J, Joshi SB, Haynes JR, Dokken L, Richardson C, Middaugh CR. H1N1 influenza virus-like particles: physical degradation pathways and identification of stabilizers. *J Pharm Sci*. 2011;100(2):634-645.
54. Liu J, Blasie CA, Shi S, Joshi SB, Middaugh CR, Volkin DB. Characterization and stabilization of recombinant human protein pentraxin (rhPTX-2). *J Pharm Sci*. 2013;102(3):827-841.
55. Shi S, Liu J, Joshi SB, et al. Biophysical characterization and stabilization of the recombinant albumin fusion protein sEphB4-HSA. *J Pharm Sci*. 2012;101(6):1969-1984.
56. Plieskatt JL, Rezende WC, Olsen CM, et al. Advances in vaccines against neglected tropical diseases: enhancing physical stability of a recombinant hookworm vaccine through biophysical and formulation studies. *Hum Vaccin Immunother*. 2012;8(6):765-776.
57. Alsenaidy MA, Wang T, Kim JH, et al. An empirical phase diagram approach to investigate conformational stability of "second-generation" functional mutants of acidic fibroblast growth factor-1. *Protein Sci*. 2012;21(3):418-432.